A role for a lithium-inhibited Golgi nucleotidase in skeletal development and sulfation

Joshua P. Frederick*, A. Tsahai Tafari*, Sheue-Mei Wu*†, Louis C. Megosh*, Shean-Tai Chiou*, Ryan P. Irving*, and John D. York*‡

*Department of Pharmacology and Cancer Biology, Howard Hughes Medical Institute, and †Department of Psychiatry and Behavioral Sciences, Duke University Medical Center, Durham, NC 27710

This Feature Article is part of a series identified by the Editorial Board as reporting findings of exceptional significance.

Edited by Philip W. Majerus, Washington University School of Medicine, St. Louis, MO, and approved June 23, 2008 (received for review February 6, 2008)

Sulfation is an important biological process that modulates the function of numerous molecules. It is directly mediated by cytosolic and Golgi sulfotransferases, which use 3′-phosphoadenosine 5′-phosphosulfate to produce sulfated acceptors and 3′-phosphoadenosine 5′-phosphate (PAP). Here, we identify a Golgi-resident PAP 3′-phosphatase (gPAPP) and demonstrate that its activity is potently inhibited by lithium *in vitro*. The inactivation of *gPAPP* in mice led to neonatal lethality, lung abnormalities resembling atelectasis, and dwarfism characterized by aberrant cartilage morphology. The phenotypic similarities of gPAPP mutant mice to chondrodysplastic models harboring mutations within components of the sulfation pathway lead to the discovery of undersulfated chondroitin in the absence of functional enzyme. Additionally, we observed loss of gPAPP leads to perturbations in the levels of heparan sulfate species in lung tissue and whole embryos. Our data are consistent with a model that clearance of the nucleotide product of sulfotransferases within the Golgi plays an important role in glycosaminoglycan sulfation, provide a unique genetic basis for chondrodysplasia, and define a function for gPAPP in the formation of skeletal elements derived through endochondral ossification.

chondrodysplasia | glycosaminoglycan | phosphatase | chondroitin sulfate | phosphoadenosine phosphate

The formation of bone occurs primarily through intramembranous and endochondral ossification. Intramembranous ossification is the emergence of bone directly from the mesenchyme and is responsible for the generation of flat bones. Endochondral ossification is the driving force of longitudinal extension best visualized in the growth plates of developing long bones and relies on a chondrocyte-produced cartilage template. Establishment of the cartilaginous template is a tightly ordered process that involves the function and interplay of: (*i*) specific transcription factors; (*ii*) chondrocyte-modulatory ligand pathways; (*iii*) extracellular matrix (ECM) structural proteins; (*iv*) core proteins of proteoglycans and their covalently linked glycosaminoglycans (GAGs), such as chondroitin sulfate (CS) chains; and correspondingly (*v*) gene products essential to the appropriate synthesis and sulfation of GAGs (1–7). Perturbations in a variety of genes that encode proteins in each of the above five categories have been implicated in endochondral ossification defects and commensurate development of chondrodysplasias that vary from subtle growth defects to severe dwarfism and neonatal lethality (7–9). Among the examples of altered genes that produce chondrodysplasias in humans with corresponding mouse models is the diastrophic dysplasia sulfate transporter (*DTDST*), which is essential for the delivery of extracellular inorganic sulfate into the cytoplasm allowing for subsequent intracellular sulfation reactions (1, 10, 11).

Sulfation is an important functional modification of a wide array of endogenous and xenobiotic compounds that is mediated by two structurally related sulfotransferase (SULT) families: cytosolic SULTs and Golgi resident SULTs (gSULTs). gSULTs are mostly single-pass transmembrane domain containing proteins that modify lipids, tyrosine residues of proteins, and GAGs (12–14). gSULT-mediated sulfation can alter the activity of certain signaling molecules, such as cholecystokinin, gastrin, and angiotensin II (14). It is also essential for the proper development, structure, and function of tissues such as cartilage through modulating the sequestration of growth factors and their binding to cognate receptors, as well as moderating appropriate interactions among ECM proteins, proteoglycans, and GAGs (14–17). SULTs modify acceptor moieties through the utilization of the universal sulfate donor 3′-phosphoadenosine 5′-phosphosulfate (PAPS) (Fig. 1*A*). Availability of PAPS enables SULTs to modify targets in a reaction that produces the sulfated substrate and 3′-phosphoadenosine 5′-phosphate (PAP). Although the molecular basis for PAP metabolism within the Golgi lumen is unknown, conversion of PAP to 5′-AMP within the cytoplasm is accomplished by a bisphosphate 3′-nucleotidase (annotated BPNT1 in mouse and human or RnPIP in rat) that also exhibits activity toward PAPS and inositol phosphate (IP) substrates (18–20).

BPNT1 belongs to a structurally conserved, lithium-inhibited family of small-molecule phosphomonoesterases, which in addition to glycogen synthase kinase, have been implicated as possible cellular targets of lithium, a drug used for the treatment of bipolar disease (21, 22). In humans and mice, this phosphatase family consists of seven gene products defined by a consensus active-site motif (Fig. 1*B*). Six of the seven family members have defined biochemical functions in IP signaling, energy homeostasis, and nucleotide metabolism; these include the aforementioned BPNT1, inositol polyphosphate 1-phosphatase (INPP1), fructose-1,6-bisphosphatase (FBP) 1 and 2, and myo-inositol monophosphatase (IMP) A1 and A2. Members of this phosphatase family are functionally inhibited *in vitro* and *in vivo* by clinically appropriate doses of lithium (22–24). Chronic lithium treatment reduces levels of inositol in brain through inhibition of IMPs and INPP1 (25–27), the loss of INPP1 in *Drosophila* mimics lithium-induced alterations in synaptic transmission (28), and perturbations in cytosolic 3′-nucleotidase activity have been shown to regulate lithium toxicity in yeast (29–31).

Author contributions: J.P.F., A.T.T., S.-M.W., and J.D.Y. designed research; J.P.F., A.T.T., S.-M.W., L.C.M., S.-T.C., and R.P.I. performed research; J.P.F. contributed new reagents/analytic tools; J.P.F., A.T.T., S.-M.W., L.C.M., S.-T.C., R.P.I., and J.D.Y. analyzed data; and J.P.F., A.T.T., S.-M.W., R.P.I., and J.D.Y. wrote the paper.

The authors declare no conflict of interest.

This article is a PNAS Direct Submission.

Freely available online through the PNAS open access option.

‡To whom correspondence should be addressed. E-mail: yorkj@duke.edu.

This article contains supporting information online at www.pnas.org/cgi/content/full/0801182105/DCSupplemental.

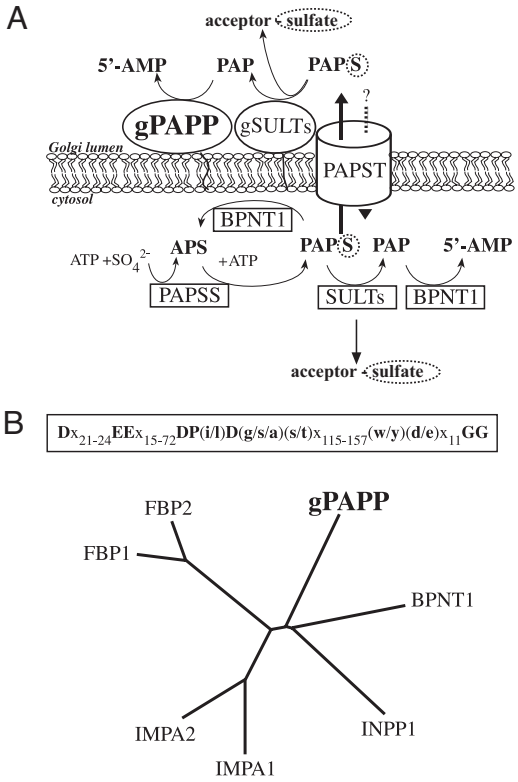

Fig. 1. The sulfation pathway including two members of a structurally conserved, lithium-sensitive phosphomonoesterase family. (*A*) Representation of acceptor sulfation mediated by cytosolic SULTs and gSULTs. The universal sulfate donor PAPS is produced in the cytoplasm by PAPS synthetases (PAPSS) from sulfate (SO_4^{2-}) and ATP through the intermediate generation of adenosine-5′-phosphosulfate (APS). PAPS can be used by SULTs in the sulfation of cytosolic small molecules or transported into the lumen of the Golgi by PAPS transporters (PAPSTs). Once luminal, PAPS is used by gSULTs in the sulfation of Golgi-restricted macromolecules. In addition to sulfate-conjugation to acceptors, sulfation produces PAP, which can be further metabolized to 5′-AMP by a predominantly cytoplasmic bisphosphate 3′-nucleotidase (BPNT1) and a gPAPP. (*B*) The consensus motif that defines the metal-dependent/lithium-sensitive phosphomonoesterase family with linking residues (X) in stretches of specified lengths is boxed. Representation of the *Mus musculus* phosphatase family is shown as an unrooted phylogentic tree produced by Clustal W and Phylip's Drawtree software. Members include FBP1 (GenBank accession no. Q9QXD6), FBP2 (GenBank accession no. P70695), IMPA1 (GenBank accession no. O55023), IMPA2 (GenBank accession no. Q91UZ5), INPP1 (GenBank accession no. P49442), BPNT1 (GenBank accession no. AAD1733), and gPAPP.

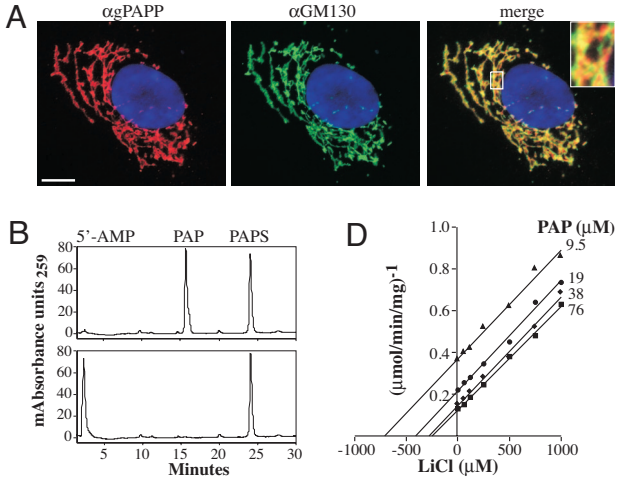

C

	K_m (μM)	V_{max} (μmole/min/mg)	K_i of LiCl (μM)
FL	21.0	9.5	174.0
Δ55	22.8	2.3	210.8

Fig. 2. Identification of gPAPP as a Golgi-resident 3′ nucleotidase inhibited by lithium. (*A*) Indirect immunofluorescence of endogenous gPAPP (red; *Left*), the known Golgi-associated GM130 (green; *Center*), and the merge of the two signals (*Right*) in normal human skin fibroblasts. gPAPP and GM130 signals partially overlap (yellow), yet higher magnification displays some distinct localization within the Golgi (*Inset*). Blue is DAPI-stained nuclei. (Scale bar: 10 microns.) (*B*) HPLC traces of resolved reaction constituents from 20 μM of PAP and PAPS treated in buffer A with no recombinant protein (Mock; *Upper*) or 200 ng of Δ55 gPAPP (*Lower*) for 1 h. 5′-AMP, PAP, and PAPS were detected by UV absorbance (259 nm) with elution times corresponding with previously run standards as indicated. Note that gPAPP treatment results in nearly complete hydrolysis of PAP to 5′-AMP, yet does not catalyze the conversion of PAPS in the used conditions. (*C*) K_m, V_{max}, and lithium K_i of PAP hydrolysis by full-length (FL) and Δ55 gPAPP purified from baculovirus-infected cells. K_m and V_{max} values were calculated from a logarithmic equation fitting average velocities obtained from at least duplicate data points plotted against various substrate concentrations. K_i of gPAPP-mediated PAP hydrolysis by LiCl are presented as the average with standard deviations calculated by the equation: $-K_i = x -$ intercept/$(1 + (K_m/[s]))$ from plotted lines obtained with each concentration of PAP used in Dixon plot analyses. (*D*) Dixon plot analysis of lithium inhibition of recombinant full-length gPAPP-mediated PAP hydrolysis. The four indicated concentrations of PAP were used to plot 1/velocity average versus inhibitor concentration, and the parallel lines signify uncompetitive inhibition.

We now report a function for the seventh member of this family as a gPAPP whose activity is inhibited by lithium *in vitro*. We find that gPAPP is required in mice for proper endochondral ossification, and its genetic inactivation results in neonatal lethality, morphological abnormalities in lung, and severe chondrodysplasia. The biochemical characterization of gPAPP and phenotypic analysis of mutant mice led to the discovery of a role for this protein in the process of GAG sulfation. Our studies provide insights into skeletal development, an unanticipated genetic basis of chondrodysplasia, and a link between loss of nucleotidase function and undersulfated molecules.

Results

gPAPP Is a Golgi Resident Protein. Murine gPAPP was first identified by searching metazoan genomes and expressed sequences for the presence of an encoded canonical active-site motif (Fig. 1*B*). We and others previously annotated this sequence in the absence of functional data as lithium-inhibited phosphomonoesterase (31), inositol monophosphatase domain containing 1 (GenBank accession no. AAH48776), and myo-inositol monophosphatase A3 (IMPA3) (GenBank accession no. AAK52336). Despite sharing nearly 20% overall sequence identity to BPNT1 and INPP1, initial attempts to identify a phosphatase activity for recombinant bacterially expressed gPAPP by using candidate nucleotide and IP substrates were unsuccessful. Further analysis of the amino acid sequence revealed a N-terminal, single-pass transmembrane domain (residues 7–29) and a consensus N-linked glycosylation sequence, N^{257}-Q-T [supporting information (SI) Fig. S1*A*], two features that raised the possibility that gPAPP may reside within the endoplasmic reticulum/Golgi. To test this hypothesis, we examined the subcellular distribution of gPAPP. Indirect immunofluorescence in normal human skin fibroblasts revealed that endogenous gPAPP was present in a perinuclear organelle that partially colocalized with the marker protein GM130, which is enriched in *cis*- but also present in *medial*- and *trans*-Golgi compartments (Fig. 2*A*). Similarly, we observed partially overlapping signals between gPAPP and the *trans*-Golgi network resident Golgin-97 (data not shown). gPAPP localization to the Golgi depended on the transmem-

brane domain and was disrupted by brefeldin A treatment, a fungal metabolite known to induce the redistribution of Golgi resident proteins (Fig. S1 *B* and *C*). Consistent with gPAPP trafficking to the distal region of the Golgi, we observed that it contained an N-linked glycan resistant to endoglycosidase H (Fig. S1*D*). This finding, in conjunction with the absence of N-linked glycosylation sites N-terminal to the transmembrane domain, indicates that gPAPP exists in a type II orientation, in which the entire catalytic core of gPAPP resides within the Golgi lumen.

***gPAPP* Encodes a Lithium-Inhibited Phosphoadenosine Phosphate 3′-Nucleotidase.** Given these results, we hypothesized that generation of functional enzyme may require luminal trafficking and/or N-linked glycosylation. Using a baculovirus-induced expression system, we produced recombinant full-length gPAPP and a secreted form that lacked the transmembrane domain (Δ55gPAPP). Based on the aforementioned sequence similarities, we then tested gPAPP for enzymatic activity toward a variety of IP and nucleotide substrates. Although insect cell-produced gPAPP failed to metabolize PAPS (Fig. 2*B*) or tested IP substrates (data not shown), it exhibited robust 3′-nucleotidase activity toward PAP (Fig. 2 *B* and *C*). We also examined the effects of lithium on gPAPP nucleotidase activity and observed an uncompetitive mode of inhibition by LiCl with an apparent K_i of near or <200 μM (Fig. 2 *C* and *D*). The kinetic parameters of gPAPP are summarized in Fig. 2*C*. Our data demonstrate that gPAPP is a selective PAP 3′-phosphatase distinct from BPNT1 with respect to compartmentalization and substrate specificity and establish this enzyme as one of the most potently inhibited targets of lithium known.

Loss of Functional gPAPP Causes Neonatal Lethality in Mice. To uncover a biological role for the Golgi-localized nucleotidase, gPAPP mutant mice were generated that no longer expressed functional protein. Two mutant embryonic stem (ES) cell clones, KST 245 and RST 634, were identified in the Bay Genomics database that incorporated gene trap vectors (32) predicted to disrupt expression of gPAPP. The RST 634 clone, which encodes the first exon of gPAPP fused to β-galactosidase, was used to generate a gPAPP mutant mouse line because it is predicted to express a truncated mutant protein that would contain only 1 of 13 catalytically conserved residues. Heterozygous mice derived from the F1 animals were grossly normal and fertile and have been maintained as a breeding colony. Molecular and biochemical analyses of WT and mutant animals demonstrate that *gPAPP*$^{gt/gt}$ mice are deficient for functional enzyme (Fig. S2 *A–D*).

Initial analyses of 275 progeny from heterozygous F2 intercross matings did not identify any living postbirth day 10 *gPAPP*$^{gt/gt}$ homozygous mutant pups, whereas WT and heterozygous pups were born at a 1:2 ratio consistent with the hypothesis that disruption of both alleles of gPAPP is either neonatal or embryonic lethal (Fig. S2*E*). To further examine the timing of the lethality, we isolated day 18.5 after coitum (E18.5) embryos and observed near Mendelian ratios of the three genotypes, indicating that *gPAPP*$^{gt/gt}$ mice were developmentally competent to reach full term of gestation (Fig. S2*E*). Observation of litter delivery revealed the live birth of animals that were subsequently genotyped as homozygous mutants. These *gPAPP*$^{gt/gt}$ mice appeared to experience severe respiratory distress and died within minutes.

Histological and gPAPP Expression Analysis of E18.5 Embryos. To gain further insights into possible causes of lethality and biological roles for gPAPP, E18.5 embryos were histologically examined, and the expression pattern of gPAPP was determined by LacZ staining for gene-trapped mutant protein (32). Frozen sagittal sections of E18.5 embryos exhibited strong expression, particularly in brain, spinal cord, and lung of homozygous mutants, approximately half the level of staining in corresponding organs of heterozygote littermates, and background signal only in the gastrointestinal tract of WTs (Fig. S3*A*). From more lateral sections, high levels of gPAPP expression were also indicated throughout kidney, including the medulla and cortex (Fig. S3*B*). Higher magnification of brain regions exhibited staining prominently in mutant neopallial cortex (Fig. S3*C*) and throughout the cerebellum with intense expression within the developing Purkinje cells and adjacent choroid plexus (Fig. S3*D*). Strong gPAPP expression was also indicated within areas of the brain that control respiration, as high levels of LacZ staining was observed in the pons and throughout the medulla oblongata (Fig. S3*E*).

Two tissues that exhibited gPAPP expression, lung and costal cartilage, also displayed gross morphological differences in the absence of functional protein. Expression was observed in individual pneumocytes and particularly in cells surrounding developing bronchi/bronchioles (Fig. S3*F*). These sections and hemotoxylin and eosin-stained paraffin-embedded tissue, exhibited small alveolar spaces and thickened septa in *gPAPP*$^{gt/gt}$ lung (Fig. S3*F* and see Fig. 6*A*). Examination of frozen sections through ribs revealed moderate LacZ staining within chondrocytes of costal cartilage and in the surrounding perichondrium (Fig. S3*G*), and Alcian blue (AB) staining of paraffin-embedded tissue demonstrated that rib cage cartilage of homozygous mutants was hypocellular with abnormal, fibrous-appearing ECM (data not shown).

Dwarfism and Anomalous Skeletal Formation in *gPAPP*$^{gt/gt}$ Mice. The most apparent differences in intact E18.5 *gPAPP*$^{gt/gt}$ embryos were reductions of limb length and a shortening of the snout (Fig. 3*A*). This observation in conjunction with the noted aberrant morphology of costal cartilage led to a closer examination of skeletal elements in homozygous mutant mice. Whole-mount staining of *gPAPP*$^{gt/gt}$ embryonic skeletons with AB and Alizarin red, which stain cartilaginous and mineralized tissue, respectively, revealed severe skeletal abnormalities in *gPAPP*$^{gt/gt}$ mice most notably in the longitudinal growth of bones formed by endochondral ossification (Fig. 3*B*). The length of the axial skeleton or trunk, measured from the top of the skull to the pelvis, was reduced in homozygous mutant mice (Fig. 3*B* and Fig. S4). The *gPAPP*$^{gt/gt}$ appendicular bones of the upper limbs (Fig. 3*C* and Fig. S4), and the ilium, femur, tibia, and fibula of the lower limbs were markedly shorter than heterozygote and WT counterparts (Fig. S4 and data not shown). The rib cages of homozygous mutant mice displayed malformation characterized by reduced sternal length and correspondingly diminished rib spacing (Fig. 3*D* and Fig. S4). In contrast, the similar size and shape of the frontal and parietal bones, and comparable lateral skull widths (Fig. 3*E* and Fig. S4), indicate that the process of intramembranous ossification is normal in mutant mice.

Chondrodysplasia Evident in Short and Disorganized *gPAPP*$^{gt/gt}$ Growth Plates. The conspicuous reduction in bones elongated by endochondral ossification prompted the histological examination of growth plates. Frozen sections of WT and *gPAPP*$^{gt/gt}$ E18.5 distal radii were stained with AB to visualize the GAG component of cartilaginous tissue and von Kossa to identify calcium deposition within bone (Fig. 4). *gPAPP*$^{gt/gt}$ growth plates exhibited reduced longitudinal zones of both epiphyseal chondrocytes (ECs), comprised of resting and proliferating chondrocytes, and columnar chondrocytes (CCs), which normally form characteristic columns of proliferating and prehypertrophic cells (Fig. 4). In contrast to the expected orientation of WT CCs forming columns parallel to the longitudinal axis, homozygous mutant cells were found to radiate laterally from the midline of the growth plate coinciding with a flared metaphysis (Fig. 4).

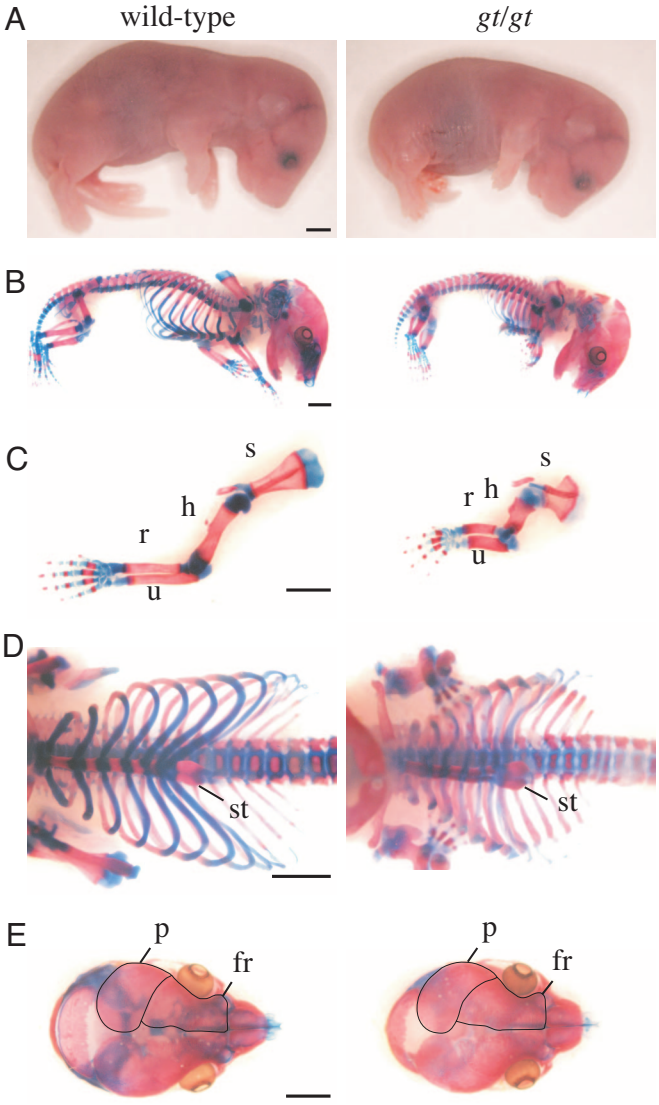

Fig. 3. Skeletal phenotype of gPAPP mutant mice. (*A*) *gPAPP*$^{gt/gt}$ E18.5 mice (*gt/gt*) (*Right*) exhibit shortened limbs compared with WT (*Left*) littermates. (*B–E*) Whole-mount preparations of WT (*Left*) and homozygous mutant (*Right*) E18.5 embryonic skeletons stained with AB and Alizarin red (AR). (*C*) Isolated forelimbs of stained embryos depicting shortened scapula (s), humerus (h), radius (r), and ulna (u) in homozygous null animals (*Right*) compared with WT (*Left*). (*D*) Increased magnification of stained rib cages, ventral view. Note reduced spacing between ribs and length of sternum (st) in *gt/gt* mice (*Right*). (*E*) Dorsal view of WT (*Left*) and *gPAPP*$^{gt/gt}$ (*Right*) AB/AR-stained skulls demonstrating similar shape and size of parietal (p) and frontal (fr) bones between genotypes (outlined in black). (Scale bars: 2 mm.)

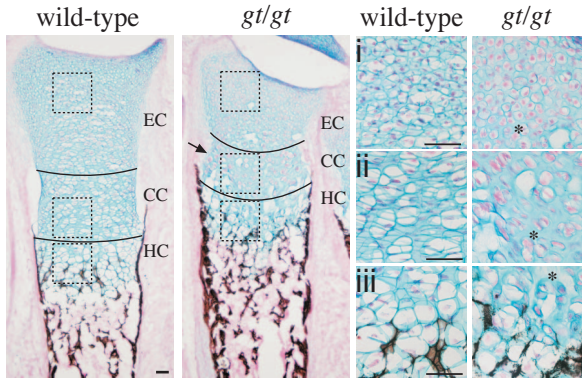

Fig. 4. Abnormalities in growth plate cartilage. Frozen sections through growth plates of distal radii of WT (*Left*) and *gPAPP*$^{gt/gt}$ (*Right*) E18.5 mice stained with AB, pH 1.0 to visualize cartilaginous tissue, von Kossa reagent for calcified bone (brown), and NFR. The overall reduced length of the homozygous mutant growth plate with particularly shortened zones of EC and CC is demonstrated. Delineation of EC, CC, and HC zones are indicated by solid arcs. Dashed boxes within EC, CC, and HC zones represent the areas of the growth plate shown magnified in *i*, *ii*, and *iii*, respectively. Relatively increased amounts of AB-positive ECM surrounding homozygous mutant chondrocytes is depicted in all three zones with large regions of acellular space particularly evident around CCs and HCs (*ii* and *iii*; ⋆). The normally longitudinal orientation of chondrocyte columns, as shown in the WT growth plate, is disrupted in the homozygous mutant growth plate (*ii*). The medial to lateral orientation of the mutant CCs corresponds with a flared metaphysis (arrow). Reduced size of mutant columnar and hypertrophic chondrocytes is shown in *ii* and *iii*. (Scale bars: 50 microns.)

LacZ staining of serial sections of mutant radii indicated gPAPP expression in the perichondrium, periostium, and throughout the growth plate with enhanced levels observed in CCs (data not shown). Higher magnification of *gPAPP*$^{gt/gt}$ ECs (Fig. 4*i*), CCs (Fig. 4*ii*), and hypertrophic chondrocytes (HCs) (Fig. 4*iii*) revealed increased regions of ECM surrounding individual cells within all layers of the growth plate, and generally smaller cell size in the columnar and hypertrophic zones. Consistent with enhanced Alizarin red staining (Fig. 3), von Kossa stain demonstrated increased mineralized collar thickness of affected bone (Fig. 4).

Deficient Sulfation of Chondroitin in *gPAPP*$^{gt/gt}$ Cartilage. Three factors led us to hypothesize that gPAPP was essential for proper chondroitin sulfation: (*i*) the similarities of chondrodysplasia-associated phenotypes in *gPAPP*$^{gt/gt}$ mice with those described in animals encoding mutations of genes known to be involved in chondroitin sulfation, (*ii*) the localization of gPAPP within the cellular compartment in which sulfation of chondroitin occurs, i.e., the Golgi, and (*iii*) the identification of PAP, a direct product of all sulfation reactions, as a gPAPP substrate. To examine possible defects in chondroitin sulfation, we stained sagittal sections of paraffin-embedded E18.5 WT and *gPAPP*$^{gt/gt}$ embryo with AB at different pHs; at pH 1.0 AB stains both weakly and strongly sulfated GAGs, whereas at pH 0.2 staining is selective for strongly sulfated GAGs (33). Consistent with a deficiency in GAG sulfation, the intensity of AB pH 1.0 stain throughout the cartilage of *gPAPP*$^{gt/gt}$ embryos was relatively similar to that observed in WT littermates, whereas AB pH 0.2 staining of mutant tissue was drastically reduced (Fig. 5*A*). To assess whether this decreased staining was caused by reduced chondroitin sulfation, we analyzed chondroitinase ABC-sensitive disaccharides released from rib cages of E18.5 littermates. Homozygous mutant cartilage exhibited a substantial decrease in chondroitin 4-sulfate (ΔDi-4S or D0a4) and an increase in nonsulfated chondroitin (ΔDi-OS or D0a0) compared with WT tissue (Fig. 5*B*). Although amounts of total disaccharides and hyaluronic acid were not statistically different between WT and homozygous mutant tissue, *gPAPP*$^{gt/gt}$ cartilage showed a ΔDi-4S reduction of 61%, a minor decrease in ΔDi-6S (or D0a6), and a corresponding 3.3-fold increase of ΔDi-OS (Fig. 5*C*). These data demonstrate that the primary detected disaccharide in WT cartilage is ΔDi-4S, normally produced by the gSULT chondroitin-4-SULT (C4ST), whereas its precursor ΔDi-OS predominates in *gPAPP*$^{gt/gt}$ tissue.

Morphologically Aberrant gPAPP Mutant Lung Exhibits Alterations in Levels of both CS and Heparan Sulfate (HS) Species. The observed abnormal architecture of *gPAPP*$^{gt/gt}$ lung (Fig. S3*F* and Fig. 6*A*) was similar to a reported atelectasis in newborn mice mutant for

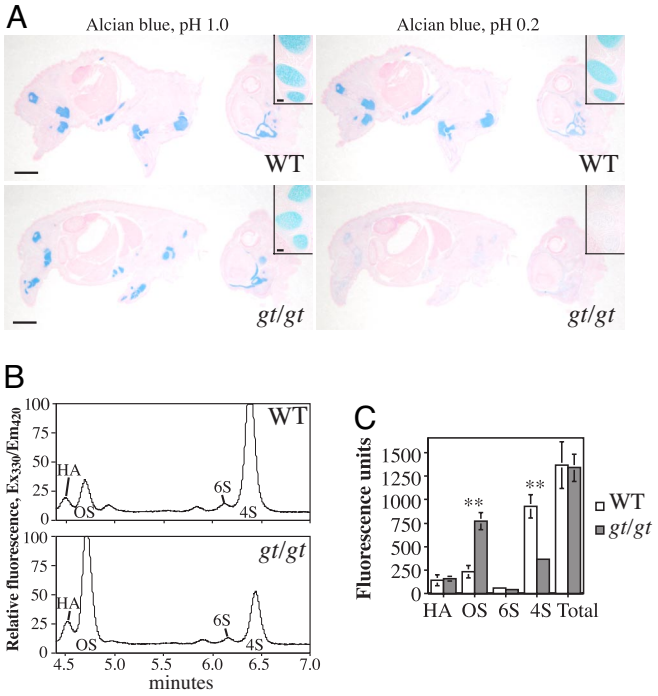

Fig. 5. Reduced chondroitin sulfation in *gPAPP*$^{gt/gt}$ cartilage. (*A*) Serial sagittal sections of paraffin-embedded WT (*Upper*) and *gPAPP*$^{gt/gt}$ (*gt/gt*; *Lower*) E18.5 embryos stained with AB, pH 1.0/NFR (*Left*) and AB, pH 0.2/NFR (*Right*). The intensity of pH 1.0 AB staining of cartilaginous tissue is relatively similar between genotypes, whereas staining of homozygous mutant cartilage with the lower pH AB is largely absent compared with WT. (Scale bars: 2 mm.) (*Insets*) Higher magnification of costal cartilage. (Scale bar: 100 microns.) (*B*) HPLC traces of chondroitinase ABC-released disaccharides recovered from equivalent wet weight amounts of E18.5 WT (*Upper*) and *gPAPP*$^{gt/gt}$ (*gt/gt*; *Lower*) rib cage starting material. Samples were fluorophore-labeled, and disaccharides were detected with 330-nm excitation (Ex)/420-nm emission (Em). Chondroitinase ABC-specific peaks of released disaccharide units from hyaluronic acid (HA), nonsulfated chondroitin (OS or D0a0), chondrotin 6-sulfate (6S or D0a6), and chondrotin 4-sulfate (4S or D0a4) were eluted at the indicated times corresponding with previously run standards. (*C*) Fluorescent units of HA, OS, 6S, and 4S disaccharides were quantified by integration of appropriate HPLC peaks from two WT and two homozygous mutant (*gt/gt*) rib cage samples in duplicate, and data are presented as averages with standard deviations. Values derived from the sum of the four detected disaccharides (Total) are shown for each genotype. Statistically different disaccharide amounts determined by unpaired Student's *t* test between genotypes are denoted by asterisks (**, $P < 0.0002$).

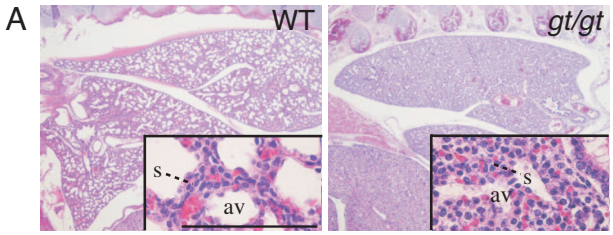

B

HS	D0A0	D0A6	D0S0/ D2A0	D0S6/ D2A6	D2S0	D2S6
Embryo						
wild-type	40.7±0.5	7.4±0.4	35.1±0.1	4.7±0.1	7.2±0.1	4.9±0.1
gt/gt	39.9±0.6	6.8±0.1	38.0±0.6	6.2±0.5	5.2±0.1	3.8±0.6
Lung						
wild-type	43.3±0.7	5.6±0.6	36.0±1.5	3.6±0.4	10.4±0.2	n.d
gt/gt	48.2±1.0	6.8±0.3	31.1±0.6	5.5±0.1	7.2±0.7	n.d.

CS	D0a0	D0a6	D0a4
Embryo			
wild-type	10.4±0.3	1.7±0.3	87.9±0.7
gt/gt	38.4±0.6	2.5±0.5	59.0±0.1
Lung			
wild-type	21.9±0.6	12.4±0.2	65.7±0.8
gt/gt	35.1±2.3	18.5±3.9	46.5±1.6

Fig. 6. Aberrant lung morphology resembling atelectasis and altered HS and CS composition in gPAPP mutant tissue. (*A*) Hemotoxylin and eosin staining of WT (*Left*) and homozygous mutant (*gt/gt*) (*Right*) paraffin-embedded E18.5 lungs. (*Insets*) Higher magnification of lung. Note decreased alveolar (av) spaces and thickened septum (s) in *gPAPP*$^{gt/gt}$ tissue. (Scale bar: 100 microns.) (*B*) HS (*Upper*) and CS (*Lower*) disaccharide constituents from WT and *gPAPP*$^{gt/gt}$ E18.5 whole embryos and isolated lungs are presented as indicated. The HS disaccharides include D0A0 or ΔUA-GlcNAc, D0A6 or ΔUA-GlcNAc6S, D0S0 or ΔUA-GlcNS, D2A0 or ΔUA2S-GlcNAc, D0S6 or ΔUA-GlcNS6S, D2A6 or ΔUA2S-GlcNAc6S, D2S0 or ΔUA2S-GlcNS, and D2S6 or ΔUA2S-GlcNS6S. Analyzed CS disaccharides are D0aO or ΔUA-GalNAc, D0a6 or ΔUA-GalNAc6S, and D0a4 or ΔUA-GalNAc4S. Data were obtained via HPLC analyses of fluorescent-labeled material, and values are presented as mean percent of total disaccharides (D0A0, D0A6, D0S0, D2A0, D0S6, D2A6, D2S0, and D2S6 for HS species and D0a0, D0a6 and D0a4 for CS). Standard deviations are shown from at least two independent samples of each genotype. Shorthand nomenclature of glycosamonoglycan standards conforms to conventions published by Lawrence *et al.* (57).

GlcNAc *N*-deacetylase/*N*-SULT-1 (Ndst-1) (34, 35). Ndst-1 is required for normal N-sulfation of HS, a GAG distinct from CS that is relatively abundant in lung. This observation in part prompted the exploration of whether gPAPP played a more global role in GAG sulfation beyond its demonstrated function in cartilage chondroitin modification. Thus, CS and HS disaccharide constituents of GAG pools purified from E18.5 whole embryos and isolated lungs were analyzed by HPLC (traces depicted in Fig. S5). The total amount of sulfated versus nonsulfated (sulfated/nonsulfated) chondroitin disaccharides normalized to wet weight of starting material recovered from WT and mutant embryos was 8.6 and 1.6, respectively. CS from isolated mutant lung also displayed decreased levels of ΔDi-4S with relatively elevated amounts of nonsulfated chondroitin (Fig. S5 and Fig. 6*B*), and the total amount of sulfated versus nonsulfated CS disaccharides was 3.6 from WT and 1.9 from mutant lung. The HS changes we observed did not recapitulate those reported for *Ndst-1* mutant tissues (36, 37) and there was not an appreciable difference in total sulfated versus nonsulfated HS disaccharides recovered from whole WT and *gPAPP*$^{gt/gt}$ embryo samples (1.5 for each genotype). However, the amount of sulfated versus nonsulfated HS disaccharides was 1.3 in WT compared with 1.1 in *gPAPP*$^{gt/gt}$ lung, signifying a small decrease in total sulfated with corresponding increase of nonsulfated HS in mutant lung. In addition, the pattern of HS species within both whole embryo- and lung-derived GAG pools exhibited alterations in the absence of gPAPP, including a notable decrease in D2S0 (Fig. S5 and Fig. 6*B*).

Discussion

Our data define an enzymatic function for a member of the structurally conserved lithium-inhibited family as a Golgi-resident PAP phosphatase and demonstrate its role as an unanticipated modulator of sulfation and skeletal development. The marked reduction in length of bones formed through endochondral ossification and the normal development of bone derived from intramembranous ossification in *gPAPP*$^{gt/gt}$ mice suggested a specific defect in the cartilage template. Taken with the aberrant morphology of developing mutant cartilage, our work provides a basis for a genetically distinct mouse model of chondrodysplasia associated with deficient chondroitin sulfation. Although human mutations in gPAPP have not been reported to

our knowledge, it is possible that unmapped cases that display short-limbed chondrodysplasia with flared metaphyses and thickened bone collars phenotypically similar to the *gPAPP*$^{gt/gt}$ mutant mouse may be attributable to gPAPP genomic or functional alteration. We now add gPAPP to a list of genes, additionally comprised of *DTDST*, *PAPSS2*, *C6ST1*, and *C4ST1* (11, 38–41) that exemplify the importance of proper sulfation in endochondral ossification, and furthermore describe a PAP phosphatase that is critically involved in metazoan sulfation.

The most dramatic assessed sulfation affect was a reduction in chondroitin 4-*O*-sulfate, generated in mice and humans by two to three distinct C4st gene products, and this defect in the primary disaccharide component of normal cartilage was correlative with the most evident phenotype, chondrodysplasia. Interestingly, there is a striking phenotypic similarity between *gPAPP*$^{gt/gt}$ and *C4st1*$^{gt/gt}$ mice in regard to neonatal lethality and exhibited skeletal abnormalities (38, 42). The long bones in both chondrodrodyplastic models exhibit shortened EC and CC zones (tissue that exhibits both gPAPP and C4st1 expression), increased amounts of abnormal ECM surrounding chondrocytes, increased collar thicknesses, and radially oriented CCs. Although these marked similarities may suggest that gPAPP only affects chondroitin 4-*O*-sulfation, we also demonstrate that HS species are altered in selected *gPAPP*$^{gt/gt}$ tissue. Thus, the presented differences in CS or HS or both may contribute to the etiological basis of the described pathology in gPAPP mutant mice. Importantly, the finding that gPAPP affects levels of both CS and HS species expands the role of this phosphatase in glycosaminogylcan sulfation, a role that may prove to be even further extended to sulfation of other carbohydrates, lipids, and proteins.

How might gPAPP play an important role in GAG sulfation? Two possible general mechanisms supported in the literature are: (*i*) gPAPP and its enzymatic activity may be necessary to clear PAP, the accumulation of which may otherwise inhibit subsequent sulfation or other cellular processes; and (*ii*) gPAPP activity is required to produce a biologically active metabolite, such as 5′-AMP, that may function as a positive regulator of sulfation, for example, as an antiporter to stimulate PAPS transport into the Golgi. First, it is well established that the product of sulfation, PAP, is capable of binding SULTs; indeed, PAP-agarose has often been used to purify these enzymes. Furthermore, it has been demonstrated that PAP, yet not 5′-AMP, acts as a potent competitive inhibitor of PAPS-mediated sulfation of dopamine and phenol by SULT1A3 and SULT1A1, respectively (43). In addition, PAP plays a critical role in substrate inhibition of SULT1A1 through the formation of a nonproductive SULT/estradiol/PAP complex, and it has been proposed that this mechanism of inhibition may be applicable to SULTs in general (44). It has also been reported in budding yeast that loss of cytosolic 3′-nucleotidase activity results in accumulation of PAP and inhibition of cellular processes (30, 31, 45). With respect to the second possible mechanism, complications arise from the uncertainty in what provides the driving force for PAPS transport from the cytoplasm into the Golgi. The transport of several nucleotide sugars and ATP into the Golgi lumen is known to occur through an antiport mechanism with corresponding nucleoside monophosphates (and/or diphosphate in the case of ATP) acting as the effluxed molecule. It has been proposed that PAPSTs use similar mechanisms (46); however, the identification of the antiporter molecule has been elusive (47–49). It is possible that gPAPP activity enhances transport of PAPS by the generation of an antiporter, such as 5′-AMP, or a downstream metabolite, or through the selective clearance of Golgi PAP it may provide a gradient enhancing the flow of PAPS into the lumen.

Further study will be necessary to delineate whether either or both of these processes are relevant to how gPAPP alters sulfation on a mechanistic level and will also assist in determining why various sulfated GAG species are differentially influenced by gPAPP function. It is interesting that gPAPP inactivation does not result in universal decreases in all sulfated GAG disaccharides, as the magnitude of CS D0a4 and HS D2S0 reduction is not observed for other detected species. The extent of gPAPP influence on GAG sulfation likely depends on multiple factors, including: (*i*) the metabolic load of specific sulfation reactions and thus how the consumption of PAPS by one gSULT may influence that of another, (*ii*) the inherent kinetic properties of individual gSULTs, (*iii*) the relative availability of PAPS and sulfate-acceptor substrates, (*iv*) tissue and cell expression patterns of gPAPP and the various gSULTs, and (*v*) possible compensation by other phosphatases.

As the seventh member of the lithium-inhibited, structurally conserved phosphatase family, the assignment of an enzyme activity to gPAPP now completes the functional tree. Within this family, gPAPP represents the only member whose catalytic domain resides in a luminal compartment and whose presumptive orthologs are found in metazoans, but not bacteria, fungi, or plants (see *SI Text*). Interestingly, gene products involved in the biosynthesis of CS and HS are also limited to metazoans (50, 51), providing a correlative argument that gPAPP may have evolved coincidently with these genes as a critical modulator of GAG sulfation. The finding that gPAPP affects Golgi-restricted sulfation also provides a foundation for the hypothesis that its predominantly cytoplasmic homolog, BPNT1, may modulate sulfation by cytosolic SULTs, such as in the modification of endogenous and xenobiotic small molecules, including neurosteroids, peripheral steroids, catecholamines, various other hormones, and pharmaceuticals. The numerous targets of sulfation that may be influenced by these nucleotidases coupled with the demonstration that they represent two of the most potently lithium-inhibited *in vitro* enzymatic activities reported to date raises the possibility that lithium may alter sulfation patterns.

Materials and Methods

Immunofluorescence. CCD-1138Sk fibroblasts grown on coverslips were fixed with methanol, rinsed in PBS supplemented with 0.1% Tween-20 (PBS-T), and then incubated with anti-gPAPP sera and mouse anti-GM130 antibody (BD Biosciences). The gPAPP antibody was raised in rabbits against peptide antigen corresponding to residues 347–359 from the *Homo sapiens* gPAPP sequence (VRKLPDLEKTGHK; 11 of which are identical in the mouse protein). The cells were again washed in PBS-T before and after incubation with secondary antibodies Alexa 488 donkey anti-mouse and Alexa 594 donkey anti-rabbit (Invitrogen). Labeled cells were mounted with DAPI-containing ProLong Gold (Invitrogen) and visualized on a Nikon TE2000 microscope.

Enzyme Kinetic and Inhibition Assays. Recombinant gPAPP protein production using a baculovirus system and its purification is described in *SI Text*. Purified recombinant Δ55 gPAPP was tested for phosphomonoesterase activity under two conditions: (*i*) buffer A [50 mM Bis·Tris (pH 6.5), 10 mM Hepes (pH 7.5), 50 μM $MnCl_2$, 0.6 mM $MgCl_2$, 90 mM KCl] and (*ii*) buffer B [60 mM Hepes (pH 7.5), 3.6 mM $MgCl_2$, 110 mM KCl and 1 mM EGTA]. Radioassays of I(1)P, I(1,4)P_2, I(1,3,4)P_3, I(1,4,5)P_3, and I(1,3,4,5)P_4 were performed at 2 nM concentration for 1 h at 37°C by using 344 ng of recombinant Δ55 gPAPP and 80 ng/μl of BSA carrier. Reactants were then evaluated by either Dowex (AG 1-X8 resin; BioRad) chromatography or HPLC methods as described (52, 53). Commercial preparations of PAPS (Sigma) contained lithium salt, which was removed by Sephadex G-10 (Amersham) filtration as described (20). Activity of Δ55 gPAPP toward PAP, PAPS, or both was tested as above at indicated concentrations of substrate. Reactions were halted by addition of 10 mM ammonium phosphate (AP), pH 3.5, and then separated by Partisphere SAX-HPLC using a linear gradient of 10 mM to 1.024 M AP over 50 min and constant 1.024 M AP over 10 min. Adenosine-containing molecules (5′-AMP, PAP, APS, and PAPS) were detected by A259, and identity was confirmed by coelution with known standards. For all analyses described above, each substrate was also tested by using recombinant INPP, IMP, or BPNT1 enzyme as positive controls.

A PAP radioassay was used for determination of gPAPP Michaelis-Menten (M-M) kinetic parameters. Briefly, 6.9 ng of Δ55 gPAPP was incubated in buffer A including 80 ng/μl BSA at 37°C with various concentrations of cold PAP and

10,000 dpm of ^{32}[P]-labeled PAP that was synthesized as described (20). Reactions were terminated with formate buffer and separated by Dowex chromatography, and [^{32}P]-5′-AMP product was quantified as described (20). The activity of full-length gPAPP on PAP was evaluated as described above, except that enzyme was preincubated with 0.25% Triton X-100 and 0.25% phosphatidylcholine on ice for 10 min, and reactions were carried out in 50 mM Bis·Tris (pH 6.5), 50 μM $MnCl_2$, 100 mM KCl, 0.1% Triton X-100, and 0.1% phosphatidylcholine. The presented K_m and V_{max} figures were determined by fitting data through the use of SigmaPlot into the M-M equation $v = V_{max}[S]/(K_m+[S])$ and using nonlinear regression analysis. The K_i and mode of inhibition of LiCl with respect to PAP hydrolysis by both Δ55 and full-length gPAPP was determined by Dixon plot analyses.

Histology and Staining. Timed-pregnant females with E18.5 litters were euthanized with an overdose of pentobarbital sodium (Abbott Laboratories), followed by β-galactosidase fixative [0.1% gluteraldehyde, 1.5% formaldehyde, 5 mM EGTA (pH 8.0), 2 mM $MgCl_2$, 100 mM sodium phosphate (pH 8.0)] transcardially perfused. Tails were removed for genotyping, and embryos were equilibrated overnight in 30% sucrose, 0.1 M phosphate buffer, pH 7.4. Embryos and limbs frozen in Tissue-Tek OCT compound (Sakura) were sectioned with a Leica CM 3050S cryostat onto gelatin-coated slides. Frozen embryo and limb sections were air-dried, fixed in 0.2% gluteraldehyde/PBS, washed, and then stained at 37°C with 1 mg/ml X-Gal (Invitrogen), 5 mM $K_4Fe(CN)_6$, 5 mM $K_3Fe(CN)_6$ in 2 mM $MgCl_2$, 0.02% Nonidet P-40, 0.01% deoxycholate, and 100 mM sodium phosphate, pH 8.0 for 24 and 44 h, respectively. Stained sections were washed with PBS and fixed in formalin overnight at 4°C, and embryo samples were counterstained with Nuclear Fast Red (NFR; Vector). Serial limb sections were also stained with von Kossa, AB 8GX (pH 1.0), and NFR. Briefly, sections through distal radii were fixed in 4% paraformaldehyde for 5 min, placed in 1% silver nitrate under UV light for 20 min, then incubated with 5% sodium thiosulfate with intervening H_20 washes. Sections were then stained in AB, pH 1.0 (1% AB in 0.1 M HCl) and counterstained in NFR. Paraffin-embedded sections of E18.5 embryos were prepared and hematoxylin and eosin-stained by the Duke University Medical Center Immunohistology Research Laboratory. Serial, paraffin-embedded sections of E18.5 mice were stained with AB at different pHs essentially as described (33) and NFR-counterstained. Briefly, paraffin was removed, and sections were rehydrated and then stained for 15 min with 1% AB in either 0.1 M HCl (pH 1.0) or 10% sulfuric acid (pH 0.2). The sections stained with AB, pH 0.2 were then rinsed in 10% sulfuric acid and blot-dried. All sections were dehydrated, cleared in Histo-Clear (National Diagnostics), and mounted with Krystalon (EMD). AB/Alizarin red staining of skeletons were performed as described (54). Bone measurements from three skeletons were made with digital calipers (L.S. Starrett) and the averages were presented. Histological reagents were obtained from Sigma unless otherwise noted.

GAG Analysis. GAG isolation and analysis is described in detail in *SI Text*.

Rib cage CS. Briefly, rib cages of E18.5 littermates were homogenized and digested with chondroitinase ABC (Seikagaku). Released disaccharides were purified, fluorophore-labeled with a GlycoProfile 2-AB labeling kit (Sigma), and resolved by HPLC using a Supelcosil LC-NH_2 250 × 4.6-mm column and linear gradient of sodium phosphate, pH 6.5. Peak identity was confirmed by coelution with known standards and ΔDi-4S susceptibility to chondro-4-sulfatase.

Whole embryo and lung GAGs. E18.5 litters were euthanized, and individual embryos were either processed whole or individual organs were isolated for homogenization. E18.5 embryos were pulverized by using a liquid nitrogen freezer mill, and isolated lungs were homogenized by hard-tissue generator. GAGs were purified from the homogenized tissue, then treated and analyzed essentially as described (55) with modifications as detailed in *SI Text*. Results are presented as a ratio of total sulfated disaccharides versus nonsulfated disaccharides (sulfated/nonsulfated as well as percent of total disaccharide detected), and the values were obtained from integrated fluorescent HPLC peaks (as depicted in Fig. S5) normalized to wet weight of starting material.

Note. During the completion of our study we became aware of a report that validated the use of alternative gene trap vectors in the generation of 60 mouse lines mutant for secreted/transmembrane gene products, including one harboring ''insertion in a novel membrane protein with similarity to inositol monophosphates'' (56). Craniofacial abnormalities and shortened limbs were noted in these mice generated from the aforementioned KST 245 ES clone, which can now be designated as mutant gPAPP. Further study of the KST245-derived line has recently been published by Sohaskey, *et al*. (58).

ACKNOWLEDGMENTS. We thank B. Hudson, B. Mutamba and Dr. W. Bai for technical assistance; Drs. I. Esko and J. Liu, and members of J.D.Y.'s laboratory, especially S. Rozenman, for helpful discussions; Drs. J. Esko, R. Lawrence (University of California San Diego, La Jolla, CA), and C. Nicchitta (Duke University Medical Center, Durham, NC) for providing reagents; and Drs. P. Majerus, S. York, and S. Kornfeld for critical reading of the manuscript and constructive comments. This work was supported by funds from the Howard Hughes Medical Institute and the National Institutes of Health R01 grant number HL-55672.

1. Schwartz NB, Domowicz M (2002) Chondrodysplasias due to proteoglycan defects. *Glycobiology* 12:57R–68R.
2. Mundlos S, Olsen BR (1997) Heritable diseases of the skeleton. Part II: Molecular insights into skeletal development-matrix components and their homeostasis. *FASEB J* 11:227–233.
3. Mundlos S, Olsen BR (1997) Heritable diseases of the skeleton. Part I: Molecular insights into skeletal development-transcription factors and signaling pathways. *FASEB J* 11:125–132.
4. Knudson CB, Knudson W (2001) Cartilage proteoglycans. *Semin Cell Dev Biol* 12:69–78.
5. Lefebvre V, Smits P (2005) Transcriptional control of chondrocyte fate and differentiation. *Birth Defects Res C Embryo Today* 75:200–212.
6. Goldring MB, Tsuchimochi K, Ijiri K (2006) The control of chondrogenesis. *J Cell Biochem* 97:33–44.
7. Cohen MM, Jr (2006) The new bone biology: Pathologic, molecular, and clinical correlates. *Am J Med Genet A* 140:2646–2706.
8. Superti-Furga A, Bonafe L, Rimoin DL (2001) Molecular-pathogenetic classification of genetic disorders of the skeleton. *Am J Med Genet* 106:282–293.
9. Horton WA (2003) The evolving definition of a chondrodysplasia? *Pediatr Pathol Mol Med* 22:47–52.
10. McLean W, Olsen BR (2001) Mouse models of abnormal skeletal development and homeostasis. *Trends Genet* 17:S38–S43.
11. Forlino A, *et al.* (2005) A diastrophic dysplasia sulfate transporter (SLC26A2) mutant mouse: Morphological and biochemical characterization of the resulting chondrodysplasia phenotype. *Hum Mol Genet* 14:859–871.
12. Kusche-Gullberg M, Kjellen L (2003) Sulfotransferases in glycosaminoglycan biosynthesis. *Curr Opin Struct Biol* 13:605–611.
13. Honke K, Taniguchi N (2002) Sulfotransferases and sulfated oligosaccharides. *Med Res Rev* 22:637–654.
14. Strott CA (2002) Sulfonation and molecular action. *Endocr Rev* 23:703–732.
15. Gama CI, *et al.* (2006) Sulfation patterns of glycosaminoglycans encode molecular recognition and activity. *Nat Chem Biol* 2:467–473.
16. Silbert JE, Sugumaran G (2002) Biosynthesis of chondroitin/dermatan sulfate. *IUBMB Life* 54:177–186.
17. Esko JD, Selleck SB (2002) Order out of chaos: Assembly of ligand binding sites in heparan sulfate. *Annu Rev Biochem* 71:435–471.
18. Ramaswamy SG, Jakoby WB (1987) (2′)3′,5′-Bisphosphate nucleotidase. *J Biol Chem* 262:10044–10047.
19. Lopez-Coronado JM, Belles JM, Lesage F, Serrano R, Rodriguez PL (1999) A novel mammalian lithium-sensitive enzyme with a dual enzymatic activity, 3′-phosphoadenosine 5′-phosphate phosphatase, and inositol-polyphosphate 1-phosphatase. *J Biol Chem* 274:16034–16039.
20. Spiegelberg BD, Xiong JP, Smith JJ, Gu RF, York JD (1999) Cloning and characterization of a mammalian lithium-sensitive bisphosphate 3′ nucleotidase inhibited by inositol 1,4-bisphosphate. *J Biol Chem* 274:13619–13628.
21. York JD, Ponder JW, Majerus PW (1995) Definition of a metal-dependent/Li(+)-inhibited phosphomonoesterase protein family based upon a conserved three-dimensional core structure. *Proc Natl Acad Sci USA* 92:5149–5153.
22. Gould TD, Quiroz JA, Singh J, Zarate CA, Manji HK (2004) Emerging experimental therapeutics for bipolar disorder: Insights from the molecular and cellular actions of current mood stabilizers. *Mol Psychiatry* 9:734–755.
23. Phiel CJ, Klein PS (2001) Molecular targets of lithium action. *Annu Rev Pharmacol Toxicol* 41:789–813.
24. Harwood AJ (2005) Lithium and bipolar mood disorder: The inositol-depletion hypothesis revisited. *Mol Psychiatry* 10:117–126.
25. Allison JH, Boshans RL, Hallcher LM, Packman PM, Sherman WR (1980) The effects of lithium on myo-inositol levels in layers of frontal cerebral cortex, in cerebellum, and in corpus callosum of the rat. *J Neurochem* 34:456–458.
26. Hallcher LM, Sherman WR (1980) The effects of lithium ion and other agents on the activity of myo-inositol-1-phosphatase from bovine brain. *J Biol Chem* 255:10896–10901.
27. Inhorn RC, Majerus PW (1987) Inositol polyphosphate 1-phosphatase from calf brain. Purification and inhibition by Li^+, Ca^{2+}, and Mn^{2+}. *J Biol Chem* 262:15946–15952.
28. Acharya JK, Labarca P, Delgado R, Jalink K, Zuker CS (1998) Synaptic defects and compensatory regulation of inositol metabolism in inositol polyphosphate 1-phosphatase mutants. *Neuron* 20:1219–1229.
29. Glaser HU, *et al.* (1993) Salt tolerance and methionine biosynthesis in *Saccharomyces cerevisiae* involve a putative phosphatase gene. *EMBO J* 12:3105–3110.
30. Dichtl B, Stevens A, Tollervey D (1997) Lithium toxicity in yeast is due to the inhibition of RNA processing enzymes. *EMBO J* 16:7184–7195.

31. Spiegelberg BD, Dela Cruz J, Law TH, York JD (2005) Alteration of lithium pharmacology through manipulation of phosphoadenosine phosphate metabolism. *J Biol Chem* 280:5400–5405.
32. Leighton PA, *et al.* (2001) Defining brain wiring patterns and mechanisms through gene trapping in mice. *Nature* 410:174–179.
33. Bancroft JD, Stevens A (1996) in *Theory and Practice of Histological Techniques* (Churchill Livingstone, New York), pp 189–191.
34. Fan G, *et al.* (2000) Targeted disruption of NDST-1 gene leads to pulmonary hypoplasia and neonatal respiratory distress in mice. *FEBS Lett* 467:7–11.
35. Ringvall M, *et al.* (2000) Defective heparan sulfate biosynthesis and neonatal lethality in mice lacking *N*-deacetylase/*N*-sulfotransferase-1. *J Biol Chem* 275:25926–25930.
36. Ledin J, *et al.* (2004) Heparan sulfate structure in mice with genetically modified heparan sulfate production. *J Biol Chem* 279:42732–42741.
37. Grobe K, *et al.* (2005) Cerebral hypoplasia and craniofacial defects in mice lacking heparan sulfate Ndst1 gene function. *Development* 132:3777–3786.
38. Kluppel M, Wight TN, Chan C, Hinek A, Wrana JL (2005) Maintenance of chondroitin sulfation balance by chondroitin-4-sulfotransferase 1 is required for chondrocyte development and growth factor signaling during cartilage morphogenesis. *Development* 132:3989–4003.
39. Thiele H, *et al.* (2004) Loss of chondroitin 6-*O*-sulfotransferase-1 function results in severe human chondrodysplasia with progressive spinal involvement. *Proc Natl Acad Sci USA* 101:10155–10160.
40. ul Haque MF, *et al.* (1998) Mutations in orthologous genes in human spondyloepimetaphyseal dysplasia and the brachymorphic mouse. *Nat Genet* 20:157–162.
41. Kurima K, *et al.* (1998) A member of a family of sulfate-activating enzymes causes murine brachymorphism. *Proc Natl Acad Sci USA* 95:8681–8685.
42. Kluppel M, Vallis KA, Wrana JL (2002) A high-throughput induction gene trap approach defines C4ST as a target of BMP signaling. *Mech Dev* 118:77–89.
43. Rens-Domiano SS, Roth JA (1987) Inhibition of M and P phenol sulfotransferase by analogues of 3′-phosphoadenosine-5′-phosphosulfate. *J Neurochem* 48:1411–1415.
44. Gamage N, *et al.* (2006) Human sulfotransferases and their role in chemical metabolism. *Toxicol Sci* 90:5–22.
45. Murguia JR, Belles JM, Serrano R (1995) A salt-sensitive 3′(2′),5′-bisphosphate nucleotidase involved in sulfate activation. *Science* 267:232–234.
46. Hirschberg CB, Robbins PW, Abeijon C (1998) Transporters of nucleotide sugars, ATP, and nucleotide sulfate in the endoplasmic reticulum and Golgi apparatus. *Annu Rev Biochem* 67:49–69.
47. Mandon EC, Milla ME, Kempner E, Hirschberg CB (1994) Purification of the Golgi adenosine 3′-phosphate 5′-phosphosulfate transporter, a homodimer within the membrane. *Proc Natl Acad Sci USA* 91:10707–10711.
48. Ozeran JD, Westley J, Schwartz NB (1996) Kinetics of PAPS translocase: Evidence for an antiport mechanism. *Biochemistry* 35:3685–3694.
49. Capasso JM, Hirschberg CB (1984) Mechanisms of glycosylation and sulfation in the Golgi apparatus: Evidence for nucleotide sugar/nucleoside monophosphate and nucleotide sulfate/nucleoside monophosphate antiports in the Golgi apparatus membrane. *Proc Natl Acad Sci USA* 81:7051–7055.
50. Perrimon N, Bernfield M (2001) Cellular functions of proteoglycans: An overview. *Semin Cell Dev Biol* 12:65–67.
51. Bishop JR, Gagneux P (2007) Evolution of carbohydrate antigens–microbial forces shaping host glycomes? *Glycobiology* 17:23R–34R.
52. Frederick JP, *et al.* (2005) An essential role for an inositol polyphosphate multikinase, Ipk2, in mouse embryogenesis and second messenger production. *Proc Natl Acad Sci USA* 102:8454–8459.
53. Inhorn RC, Majerus PW (1988) Properties of inositol polyphosphate 1-phosphatase. *J Biol Chem* 263:14559–14565.
54. Scheijen B, Bronk M, van der Meer T, Bernards R (2003) Constitutive E2F1 overexpression delays endochondral bone formation by inhibiting chondrocyte differentiation. *Mol Cell Biol* 23:3656–3668.
55. MacArthur JM, *et al.* (2007) Liver heparan sulfate proteoglycans mediate clearance of triglyceride-rich lipoproteins independently of LDL receptor family members. *J Clin Invest* 117:153–164.
56. Mitchell KJ, *et al.* (2001) Functional analysis of secreted and transmembrane proteins critical to mouse development. *Nat Genet* 28:241–249.
57. Lawrence R, Lu H, Rosenberg RD, Esko JD, Zhang L (2008) Disaccharide structure code for the easy representation of constituent oligosaccharides from glycosaminoglycans. *Nat Methods* 5:291–292.
58. Sohaskey ML, Yu J, Diaz MA, Plaas AH, Harland RM (2008) JAWS coordinates chondrogenesis and synovial joint positioning. *Development* 135:2215–2220.